

# Imprint of the stochastic nature of photon emission by electrons on the proton energy spectra in the laser-plasma interaction

Feng Wan,<sup>1</sup> Kun Xue,<sup>1</sup> Zhen-Ke Dou,<sup>1</sup> Karen Z. Hatsagortsyan,<sup>2</sup> Wenchao Yan,<sup>3,\*</sup> Danila Khikhlikha,<sup>3</sup> Sergei V. Bulanov,<sup>3,4,5</sup> Georg Korn,<sup>3</sup> Yong-Tao Zhao,<sup>1</sup> Zhong-Feng Xu,<sup>1</sup> and Jian-Xing Li<sup>1,†</sup>

<sup>1</sup>*School of Science, Xi'an Jiaotong University, Xi'an 710049, China*

<sup>2</sup>*Max-Planck-Institut für Kernphysik, Saupfercheckweg 1, 69117 Heidelberg, Germany*

<sup>3</sup>*Institute of Physics ASCR, v.v.i. (FZU), ELI BEAMLINES,  
Za Radnicí 835, Dolní Břežany, 252241, Czech Republic*

<sup>4</sup>*Kansai Photon Science Institute, National Institutes for Quantum and Radiological Science and Technology,  
8-1-7 Umemidai, Kizugawa-shi, Kyoto, 619-0215, Japan*

<sup>5</sup>*Prokhorov Institute of General Physics of the Russian Academy of Sciences, Vavilov St. 38, 119991, Moscow, Russia*

(Dated: September 9, 2022)

In QED the photon emission process is probabilistic in contrast to classical radiation theory that significantly modifies radiation reaction in ultrastrong laser fields. This fundamental property of photon emission - stochasticity effect (SEs) - can be probed in the electron-laser beam interaction via electron characteristics as shown previously theoretically, but challenging to observe experimentally. In this work we investigate theoretically SEs for the proton energy spectra during laser-plasma interaction in the quantum radiation-dominated regime, which may facilitate SEs experimental observation. An ultrarelativistic plasma generated and driven by an ultraintense laser pulse, collides head-on with counterpropagating laser pulse, which decelerates the electrons due to radiation reaction, and results in significant compression of the proton energy spectra because of the charge separation force. In the considered regime the SEs are demonstrated in the shift of the mean energy of the protons up to hundreds of MeV. The effect is robust with respect to the laser and target parameters and measurable in soon available strong laser facilities.

## I. INTRODUCTION

With the rapid development of ultrashort ultraintense laser techniques, present laser peak intensity can reach up to about  $10^{22}$  W/cm<sup>2</sup> [1–4], which can be exploited to gain new insight for fundamental physics [4–11]. In ultrastrong laser fields, the electron dynamics is ultrarelativistic and characterized by multi-photon nature [12–20]. The energy loss of an electron due to the radiation can be comparable to its own energy, greatly modifying the electron dynamics and enhancing radiation reaction (RR) effects [9, 21–25]. In the quantum radiation regime, the photon emissions are discrete and probabilistic, which leads to stochasticity effects (SEs) in electron dynamics [14, 26–31]. SEs quantitatively enhance the hard-photon emission in ultrastrong field due to, so-called, electron straggling effect [32], and in this way have significant impact on RR. It is found that SEs can quench radiation losses in subcycle PW lasers [33], and heat electron beams in plane-wave, or standing-wave laser fields [26, 27, 30]. Moreover, SEs can reshape the angular spectra of electron beams and emitted photons [28, 34, 35].

Recently, experimental evidences for quantum RR effects have been demonstrated in the radiation spectra of an ultrarelativistic positron beam traversing a silicon slab [36] and in the energy loss of an electron beam after colliding with a strong laser pulse [37, 38]. However, in

those experiments all quantum properties, including SEs and photon recoil effects, arise simultaneously. Thus, the detection of the sole signature of SEs is still a challenging and opening question.

Although RR directly disturbs the electron dynamics during laser-plasma interaction, it has indirect influence on the ion dynamics due to the charge separation quasi-static fields, which are modified by RR disturbed electron motion. Thus, RR effect can enhance the ion acceleration in the optical transparency region [39], or reduce it in dense plasma targets [40]. The reduction of the ion peak energy and of the width of energy spectrum for linearly polarized laser pulses are shown in [41]. Thus, in principle, strong SEs can also be manifested in the ion dynamics during laser-plasma interaction.

As known, SEs appear in the quantum regime when  $\chi \sim 1$ , and SEs are especially conspicuous in the, so-called, quantum radiation-dominated regime (QRDR), which requires  $R_Q \equiv \alpha a_0 \chi \gtrsim 1$  [9, 34], indicating that the radiation losses during a laser period are comparable with the electron initial energy.  $\alpha = e^2/c\hbar$  is the fine structure constant,  $\chi = e\hbar|F_{\mu\nu}p^\nu|/m^3c^4$  the quantum invariant parameter,  $\hbar$  the reduced Planck constant,  $F_{\mu\nu}$  the electromagnetic field tensor,  $p^\nu = (\varepsilon/c, \mathbf{p})$  the four-momentum of electron,  $c$  the speed of light in vacuum,  $e$  and  $m$  are the electron charge and mass, respectively.  $a_0 = eE_0/mc\omega_0$  is the invariant laser field amplitude,  $\omega_0$  the laser frequency, and  $E_0$  the laser field amplitude.

In this paper, we investigate theoretically the signature of SEs in the proton spectra during interaction of a solid plastic target with laser fields in QRDR. We consider a typical radiation pressure acceleration (RPA) scheme,

\* Wenchao.Yan@eli-beams.eu

† jianxing@xjtu.edu.cn

when a circularly-polarized ultraintense laser pulse irradiates onto a tens of nanometer solid target (e.g., the widely used polystyrene (PS)  $(C_8H_8)_n$  with an electron density about  $10^3$  times higher than the critical density [42–44]), and electrons are directly pushed out as a sheet by the light pressure [45–48]. The charge separation field between the electron and ion sheets can accelerate ions continuously until the balance between this field and the radiation pressure breaks down or the plasma instabilities strongly deform the electron sheet [47, 48]. To detect SEs, the accelerated plasma after about 19-laser-period acceleration, head-on collides with another ultraintense (scattering) laser pulse, see the scenario in Fig. 1. The electron sheet is slowed down mostly due to RR, and partially pushed back by the scattering laser pulse, resulting in disturbance on the acceleration progress of protons and compression of their momentum distribution.

We carry out optimization over the laser intensity and the pulse duration to achieve the best SE signature. First of all, in the scattering stage the condition for the QRDR regime should be fulfilled  $R_Q \gtrsim 1$  and  $\chi \sim 1$ . In the laser-electron counterpropagating configuration,  $\chi$  can be estimated as  $\chi \simeq \hbar\omega_0\gamma_e a_0/mc^2$ , where  $\gamma_e$  is the electron Lorentz factor. Employing current achievable laser pulses (the peak intensity  $I_0 \sim 10^{22} \text{W/cm}^2$  and  $a_0 \sim 10^2$ ) head-on colliding with an electron beam with a mean energy from hundreds of MeV to several GeV ( $\gamma_e \sim 10^2 - 10^3$ ) [48–54], the QRDR condition  $R_Q \gtrsim 1$  can be reached. In the optimal case the peak intensity of the driving laser pulse is  $8.5 \times 10^{22} \text{W/cm}^2$  and the length is 6 cycles, while the scattering pulse peak intensity is  $1.1 \times 10^{23} \text{W/cm}^2$  and the length is 16 cycles. The mean energies of electrons and protons are both about hundreds of MeV, and the latter is a bit higher.

We simulate the plasma dynamics through two semi-classical models based on the two-dimensional (2D) particle-in-cell (PIC) EPOCH code [55, 56]: the first considers quantum RR effects via the, so-called, modified Landau-Lifshitz (LL) equation [9, 37], which includes quantum recoil effects but not SEs; the second is a Monte-Carlo (MC) method, which includes both of quantum recoil effects and SEs [57–60]. For the given parameters our simulations show that SEs change significantly the shift of the proton energy spectra and the width of spectral distribution after scattering, which can serve as a signature of SEs. The compression of the proton energy distribution, seen previously beyond the QRDR in two-color [61] or two-intensity [62] laser setups, is shown to be significant also in QRDR.

This paper is organized as follows. In Sec. II, we present theoretical models to describe the electron dynamics including RR effects. In Sec. III, the signatures of SEs on the proton energy spectra are presented and analyzed. In Sec. IV, the impacts of laser and target parameters on the signature of SEs are discussed. Finally, the conclusion is given in Sec. V.

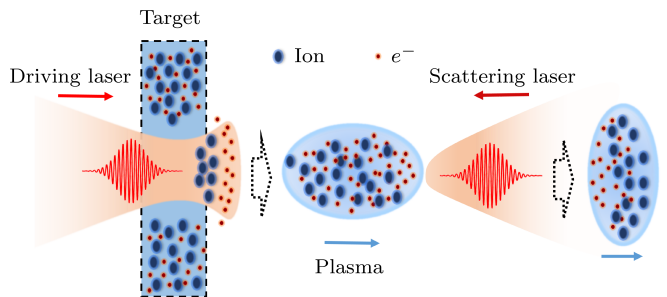


FIG. 1. Scenario of detecting SEs signatures in the proton spectra. An ultrarelativistic plasma beam consisting of electrons and ions is generated by RPA, which further head-on collides with an ultraintense scattering laser pulse. The scattering laser pulse decelerates and compresses the electrons and, consequently, the protons because of the charge separation force. As a result the proton energy spectrum shifts down, and the latter is SEs dependent.

## II. THEORETICAL MODELS

In the classical regime, i.e.,  $\chi \ll 1$ , the LL equation [63] can be employed to describe the electron dynamics including the RR effects [9]. But, as  $\chi \gtrsim 1$ , this model will overestimate the total radiation power, which is commonly handled by introducing a  $g(\chi)$  function to suppress the RR force, mimicking the effect of the quantum recoil [16, 64] (a polynomial fraction fits for  $g(\chi)$  is given in Ref. [16]). The modified LL (MLL) model includes quantum recoil effects but not SEs. However, at  $\chi \gtrsim 1$  SEs, i.e., the discrete and probabilistic characteristics of photon emission, can notably affect the electron dynamics and radiation [26, 28–30, 35]. In ultraintense laser fields,  $a_0 \gg 1$ , the coherence length of photon emission is much smaller than the laser wavelength and the typical size of the electron trajectory [15, 65]. In this regime, proper quantum theory for the electron dynamics and radiation can be implemented via the MC simulation [57–60].

### A. Modified Landau-Lifshitz (MLL) Model

In classical regime, the RR effects are considered as radiation-induced damping on the motion of charged particles. Compared with the Lorentz-Abraham-Dirac (LAD) equation, the LL equation is self-consistent and avoids the runaway solution [17, 66–68]. The dynamics of an electron is described by the LL equation [63]

$$m \frac{du^\mu}{d\tilde{\tau}} = eF^{\mu j} u_j + f^\mu, \quad (1)$$

where

$$f^\mu = \frac{2e^4}{3m^2 c^4} (F^{\mu\nu} F_{\nu\alpha} u^\alpha + (F^{\nu\beta} u_\beta F_{\nu\alpha} u^\alpha) u^\mu) + \frac{2e^3}{3mc^2} (\partial_\alpha F^{\mu\nu} u_\nu u^\alpha), \quad (2)$$

$u = (\gamma_e, \gamma_e \mathbf{v}/c)$  is four-velocity of the electron,  $\tilde{\tau}$  the proper time,

$$\frac{d}{d\tilde{\tau}} = c(k \cdot u) \frac{d}{d\tilde{\eta}}, \quad \tilde{\eta} = (k \cdot \tilde{r}), \quad (3)$$

and  $\tilde{r}$  the four-vector of the coordinate. The three-dimensional expression of Eq. (2) is

$$\begin{aligned} \mathbf{F}_{RR, classical} = & \frac{2e^3}{3mc^3} \left( \gamma_e \left( \left( \frac{\partial}{\partial t} + \frac{\mathbf{p}}{\gamma_e m} \cdot \nabla \right) \mathbf{E} + \frac{\mathbf{p}}{\gamma_e mc} \times \left( \frac{\partial}{\partial t} + \frac{\mathbf{p}}{\gamma_e m} \cdot \nabla \right) \mathbf{B} \right) \right. \\ & + \frac{e}{mc} \left( \mathbf{E} \times \mathbf{B} + \frac{1}{\gamma_e mc} \mathbf{B} \times (\mathbf{B} \times \mathbf{p}) + \frac{1}{\gamma_e mc} \mathbf{E} (\mathbf{p} \cdot \mathbf{E}) \right) \\ & \left. - \frac{e\gamma_e}{m^2 c^2} \mathbf{p} \left( \left( \mathbf{E} + \frac{\mathbf{p}}{\gamma_e mc} \times \mathbf{B} \right)^2 - \frac{1}{\gamma_e^2 m^2 c^2} (\mathbf{E} \cdot \mathbf{p})^2 \right) \right), \end{aligned} \quad (4)$$

where  $\mathbf{E}$  and  $\mathbf{B}$  are the electric and magnetic fields, respectively. To include the quantum suppression in the MLL equation, the classical RR force is replaced by the quantum modified RR force [17, 69]

$$\mathbf{F}_{RR, quantum} = q(\chi) \mathbf{F}_{RR, classical}, \quad (5)$$

where

$$q(\chi) = \frac{I_{QED}}{I_C}, \quad (6)$$

$$I_{QED} = mc^2 \int c(k \cdot k') \frac{dW_{fi}}{d\tilde{\eta} dr_0} dr_0, \quad (7)$$

$$I_C = \frac{2e^4 E'^2}{3m^2 c^3}, \quad (8)$$

$W_{fi}$  is the radiation probability, see below Eq. (9),  $r_0 = \frac{2(k \cdot k')}{3\chi(k \cdot p_i)}$ , and  $E'$  is the electric fields in the electron frame.  $k$ ,  $k'$  and  $p_i$  are the four-vector of the wave vector of the driving laser, the wave vector of the radiated photon, and the momentum of the electron before the radiation, respectively. In the MLL equation, the recoil effects are included by rescaling the RR force by the factor  $I_{QED}/I_C$ , the ratio of the radiation intensities within QED and classical approaches, which will account for the classical overestimation of the RR effects on the electron dynamics.

## B. Monte-Carlo (MC) Model

In this model, the calculation of the electron dynamics is based on the MC simulation employing QED theory for the electron radiation and classical equations of motion for the propagation of electrons between photon emission [57–60]. In superstrong laser fields,  $a_0 \gg 1$ , the photon emission probability  $W_{fi}$  is determined by the local electron trajectory, consequently, by the local value of the

parameter  $\chi$  [15]:

$$\frac{d^2 W_{fi}}{d\tilde{\eta} dr_0} = \frac{\sqrt{3}\alpha\chi [\int_{r_\chi}^\infty K_{5/3}(x) dx + N_c K_{2/3}(r_\chi)]}{2\pi\lambda_c(k \cdot p_i)}, \quad (9)$$

where the coefficient  $N_c = 9r_0 r_\chi \chi^2/4$ , the Compton wavelength  $\lambda_c = \hbar/mc$ , and  $r_\chi = r_0/(1 - 3\chi r_0/2)$ . The photon emission of electrons is considered to be a MC stochastic process [57–60]. During the electron-laser interaction, for each propagation coherent length  $\Delta\tilde{\eta}$ , the photon emission will take place if the condition  $(dW_{fi}/d\tilde{\eta})\Delta\tilde{\eta} \geq N_r$  is fulfilled, where  $N_r$  is a uniformly distributed random number in  $[0, 1]$ . Herein, the coherent length  $\Delta\tilde{\eta}$  is inversely proportional to the invariant laser field parameter  $a_0$ , i.e.,  $\Delta\tilde{\eta} \sim 1/a_0$ . However, to keep the total photon emission energy consistent, i.e., to exclude numerical error of the simulation of photon emission, we choose  $\Delta\tilde{\eta} \ll 1/a_0$ . The photon emission probability

$$W_{fi} = \Delta\tilde{\eta} \frac{dW_{fi}}{d\tilde{\eta}} = \Delta\tilde{\eta} \int_{\omega_{min}}^{\omega_{max}} \frac{d^2 W_{fi}}{d\tilde{\eta} d\omega} d\omega,$$

where  $\hbar\omega_{min}$  and  $\hbar\omega_{max}$  are assumed to equal the driving laser photon energy and the electron instantaneously kinetic energy, respectively. In addition, the emitted photon frequency  $\omega_R$  is determined by the relation:

$$\frac{1}{W_{fi}} \int_{\omega_{min}}^{\omega_R} \frac{dW_{fi}(\omega)}{d\omega} d\omega = \frac{\Delta\tilde{\eta}}{W_{fi}} \int_{\omega_{min}}^{\omega_R} \frac{d^2 W_{fi}(\omega)}{d\tilde{\eta} d\omega} d\omega = \tilde{N}_r,$$

where,  $\tilde{N}_r$  is another independent uniformly distributed random number in  $[0, 1]$ . Between the photon emissions, the electron dynamics in the laser field is governed by classical equations of motion:

$$\frac{d\mathbf{p}}{dt} = e(\mathbf{E} + \frac{\mathbf{v}}{c} \times \mathbf{B}). \quad (10)$$

Given the smallness of the emission angle  $\sim 1/\gamma_e$  for an ultrarelativistic electron, the photon emission is assumed to be along the electron velocity. The photon

emission induces the electron momentum change  $\mathbf{p}_f \approx (1 - \hbar\omega_R/c|\mathbf{p}_i|)\mathbf{p}_i$ , where  $\mathbf{p}_{i,f}$  are the electron momentum before and after the emission, respectively.

### III. RESULTS AND ANALYSIS

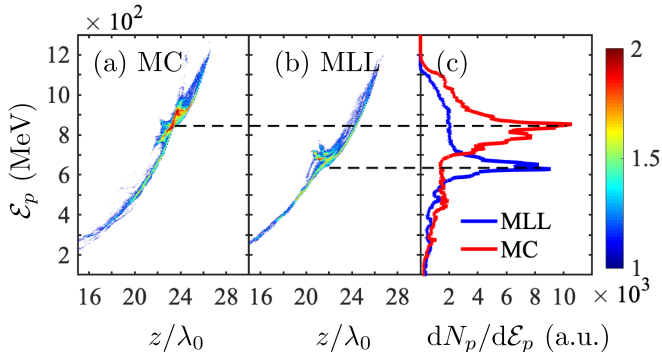


FIG. 2. (a), (b): Proton energy spectra  $\text{Log}_{10}(d^2N_p/d\mathcal{E}_p dz)$  (a.u.) with respect to the proton energy  $\mathcal{E}_p$  and  $z$  at  $t = 19T_0$  for the MC and MLL models, respectively.  $N_p$  is the proton number. The interaction between the scattering laser pulse and the accelerated plasma is assumed to start at  $t = 0$ . (c) The proton energy spectra  $dN_p/d\mathcal{E}_p$  (a.u.) with respect to the proton energy  $\mathcal{E}_p$ . The red and blue curves indicate the MC and MLL models, respectively. The laser and plasma parameters are given in the text.

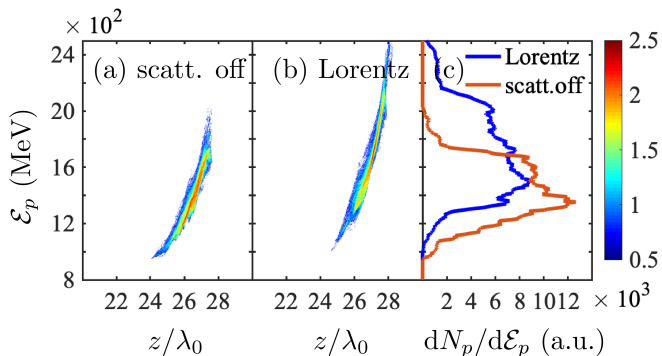


FIG. 3. (a), (b): Proton energy spectra  $\text{Log}_{10}(d^2N_p/d\mathcal{E}_p dz)$  (a.u.) with respect to  $\mathcal{E}_p$  and  $z$  excluding and including the scattering laser pulse, respectively. (c) The proton energy spectra  $dN_p/d\mathcal{E}_p$  (a.u.) with respect to the proton energy  $\mathcal{E}_p$ . The red and blue curves indicate the cases excluding and including the scattering laser pulse, respectively. In (b) and the blue curve in (c), only the Lorentz force is considered. Other parameters are the same as in Fig. 2.

In the RPA scheme, multi-species plasmas with high electron density is beneficial for acceleration [70, 71]. For the feasibility of experiments, the polystyrene (PS)  $(C_8H_8)_n$ , which can be easily manufactured in a relatively large range of density and has been widely used for laser plasma interaction [42–44], is chosen as the

target, see Fig. 1. An uniform plasma slab is chosen with an electron density  $n_0 = 300n_c$  and thickness  $l = 0.3\lambda_0$ , where  $n_c = m\omega_0^2/4\pi e^2$  is the critical density, and  $\lambda_0 = 1\mu\text{m}$  the laser wave length. Each cell is filled with 200 pseudo-electrons, 200 pseudo-protons and 100  $C^{6+}$  macro-particles. The driving laser pulse is circularly polarized with gaussian profile in the trasverse direction and 4th-order supergaussian temporal profile, propagating in the  $+z$  direction with peak intensity  $I_0 \approx 8.5 \times 10^{22} \text{W/cm}^2$  ( $a_0 \approx 250$ ), beam radius  $w_0 = 5\lambda_0$ , and pulse duration  $\tau_0 = 6T_0$ .  $T_0$  is the laser period. The scattering laser pulse is linearly polarized in the  $x$  direction with gaussian profile both in the transverse direction and temporal, propagating along the  $-z$  direction with peak intensity  $I_1 \approx 1.1 \times 10^{23} \text{W/cm}^2$  ( $a_1 \approx 286$ ), wavelength  $\lambda_1 = \lambda_0$ , beam radius  $w_1 = 5\lambda_0$ , and pulse duration  $\tau_1 = 16T_0$ . The interaction time delay between the driving laser pulse and the scattering laser pulse is about  $19T_0$ .

One set of typical simulation results is presented in Fig. 2. In the MC model including SEs, see Fig. 2(a), a very dense proton layer is accelerated to the energy at the peak proton density  $\mathcal{E}_p \approx 850$  MeV in the longitudinal range of  $23\lambda_0 \lesssim z \lesssim 25\lambda_0$ . As SEs are artificially removed in the MLL model, the energy at the peak proton density reaches only about 630 MeV, which is much lower than that in the MC model, see Fig. 2 (b). The comparison is shown in Fig. 2(c). This energy shift between the MLL and MC models can be considered as a signature of SEs on the proton energy spectra (the latter shows a higher mean energy). In both cases, the acceleration process is disturbed by the scattering laser pulse. Figure 3 indicates the roles of the scattering laser pulse and the RR effects. As the scattering laser pulse is not employed, see Figs. 3(a) and (c) (the red curve), the protons can be accelerated to a much higher energy, and the energy at the peak density is about 1.35 GeV. As the RR effects are not taken into account, as shown in Figs. 3(b) and (c) (the blue curve), the proton energy spectra is very broad and can be easily distinguished from the MLL and MC models, which confirms that the RR effects can compress the proton spectra.

As already mentioned, the scattering laser pulse can disturb the acceleration process, i.e., the balance between the electrostatic field and the light pressure. Compare Figs. 2 and 3(a): in the MLL model the down shift of the proton spectra is much larger than in the MC model, which means a larger disturbance on the acceleration process. The reason is analyzed in Fig. 4, in which the densities of electrons and protons at different times are illustrated. At the beginning of scattering, see Figs. 4(a1) and (a2), slight differences on electron dynamics in the MC and MLL models emerge already. The electron density in the region of  $-8 \lesssim z/\lambda_0 \lesssim -6$  in the MLL model (Fig. 4(a1)) is lower than in the MC model (Fig. 4(a2)) and excites different longitudinal force, see the black-dashed curves. The corresponding proton density distributions are shown in Figs. 4(b1) and (b2). For



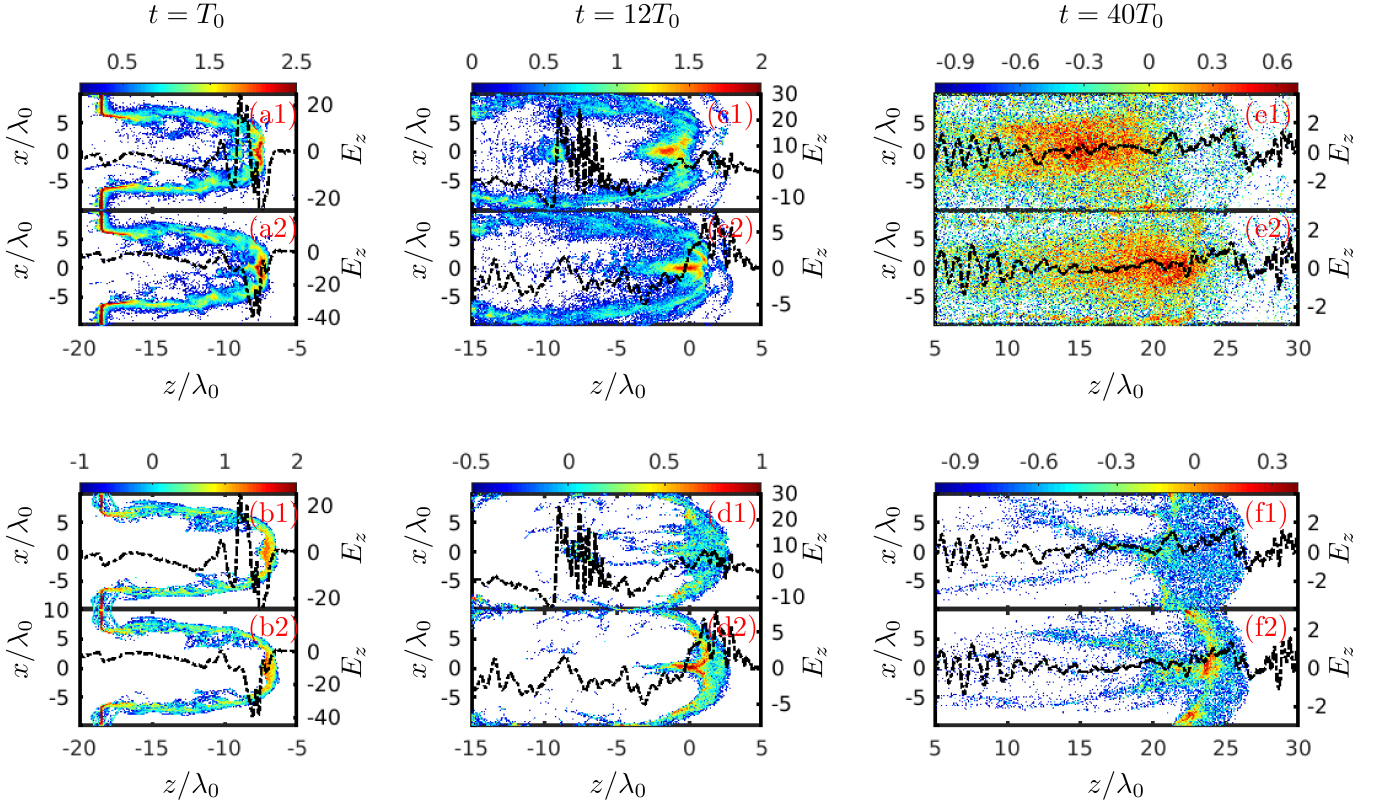


FIG. 4. (a1), (a2), (c1), (c2), (e1) and (e2): Density distribution of electrons  $\log_{10}(n_0/n_c)$ . (b1), (b2), (d1), (d2), (f1) and (f2): Density distribution of protons  $\log_{10}(n_p/n_c)$ . The black-dashed lines indicate the normalized electric field  $E_z$ . (a1)-(b2), (c1)-(d2), and (e1)-(f2) show the results at  $t = T_0$ ,  $12T_0$ , and  $40T_0$ , respectively. (a1), (b1), (c1), (e1) and (f1) are simulated via the MLL model, and (a2), (b2), (c2), (e2) and (f2) via the MC model. Other parameters are the same as in Fig. 2.

the given parameters in the MLL model more electrons can be scattered back than in the MC model due to the absence of SEs [28, 35, 72], i.e., in the MLL model the electrons can be reflected by the scattering laser pulse as the reflection condition  $\gamma_e \lesssim a_1/2$  [9] is fulfilled due to the successive radiation energy loss, however, in the MC model the electrons may emit photons or not due to SEs in the same period. Thus, due to higher penetration ratio of electrons, in the MC model the electron peak density is higher than in the MLL model, see Figs. 4(c1) and (c2) as well. More unscattered electrons can drag more protons moving forwards together due to the charge separation force, consequently, resulting in different longitudinal field distribution, see Figs. 4(d1) and (d2). After the scattering, those differences are further enhanced due to the plasma evolution, see Figs. 4(e1)-(f2). Thus, the absence of SEs in the MLL model can induce a downshift of the proton energy spectra compared with in the MC model, as shown in Fig. 2.

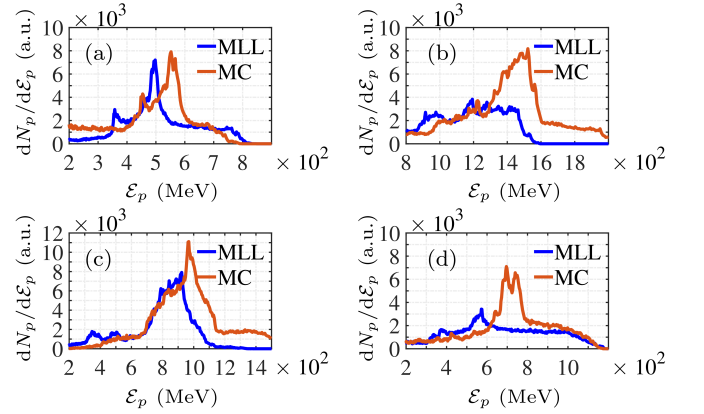


FIG. 5. Proton energy spectra at  $t = 40T_0$ . The driving laser peak intensity in (a) is  $I_0 \approx 5.4 \times 10^{22} \text{W/cm}^2$  ( $a_0 \approx 200$ ) and (b)  $I_0 \approx 1.2 \times 10^{23} \text{W/cm}^2$  ( $a_0 \approx 300$ ), respectively. The scattering laser peak intensity in (c) is  $I_1 \approx 7.7 \times 10^{22} \text{W/cm}^2$  ( $a_1 \approx 238$ ) and (d)  $I_1 \approx 1.5 \times 10^{23} \text{W/cm}^2$  ( $a_1 \approx 332$ ), respectively. Other parameters are the same as in Fig. 2.

#### IV. THE IMPACTS OF LASER AND TARGET PARAMETERS ON THE SIGNATURE OF SES

The impacts of crucial laser and target parameters on the signature of SEs on the proton energy spectra are investigated in detail. We start with the intensities of the driving laser  $a_0$  and the scattering laser  $a_1$ . As  $a_0$  and  $a_1$  match each other within a certain range, the signature of SEs can be observed via the shift of the proton energy spectra, see Fig. 5. Decreasing the driving laser intensity  $a_0$  will reduce the energy gains of electrons and protons in the RPA, consequently, SEs are suppressed due to the decrease of the parameter  $\chi \sim \gamma_e a_1$ . A sample of  $a_0 \approx 200$  is shown in Fig. 5(a). The peak energy shift between MC (about 550 MeV) and MLL (about 500 MeV) reduces to about 50 MeV, compared with in Fig. 2 ( $a_0 \approx 250$ ). For a larger  $a_0$ , on one hand, the electron energy and the parameter  $\chi$  are higher, thus, SEs are stronger; on the other hand, a larger  $a_0$  means when the scattering process is finished, the driving laser pulse can still provide acceleration, which may overwhelm SEs, see Fig. 5(b). The scattering laser intensity  $a_1$  plays a similar role as  $a_0$  for SEs. If  $a_1$  is weak, the parameter  $\chi \sim \gamma_e a_1$  for electrons is small as well, and SEs are suppressed, see the case for  $a_1 = 250$  in Fig. 5(c). On the contrary, a stronger  $a_1$  can enhance SEs, thus, more electrons can be scattered back, see the case of  $a_1 = 350$  in Fig. 5(d). Apparently, a much stronger  $a_1$  not only enhances SEs but also pushes all electrons backwards, which may submerge the signature of SEs.

The roles of the pulse durations of the driving laser  $\tau_0$  and the scattering laser  $\tau_1$  are analyzed in Fig. 6. For a shorter  $\tau_0$ , the electron energy is lower since the relevant acceleration time is shorter accordingly, thus, SEs are more difficult to be distinguished since  $\chi \sim \gamma_e a_1$ , see Fig. 6(a), in which the energy shift between MC and MLL is smaller compared with Fig. 2. For a longer  $\tau_0$ , the electrons scattered by the RR effects can be re-accelerated to high energies, SEs are also suppressed, see the sample case of  $\tau_0 = 8T_0$  in Fig. 6(b). The duration of the scattering laser pulse determines the total energies of electrons depleted by the RR effects. Shortening the pulse duration of the scattering laser can reduce the radiation and subsequent SEs, see the case of  $\tau_1 = 8T_0$  in Fig. 6(c). And, a longer  $\tau_1$  can strengthen the RR effects and also SEs, see Fig. 6(d).

Furthermore, the effects of the colliding time are analyzed in Figs. 7(a) and (b). If the colliding is delayed, the protons and electrons can be accelerated to higher energies. This leads to a stronger RR force since  $\chi \sim \gamma_e a_1$ . But, if the delay is enough for completing the acceleration process, such as the case of  $\tau_c = 10T_0$  in Fig. 7(a), the scattering laser pulse is hard to decelerate the electrons, to pose a significant impact on the proton spectra, and, consequently, to resolve SEs, although the proton densities can be easily distinguished. While, if the scattering laser pulse enters earlier, the acceleration process is disturbed earlier. This prolongs the interaction between

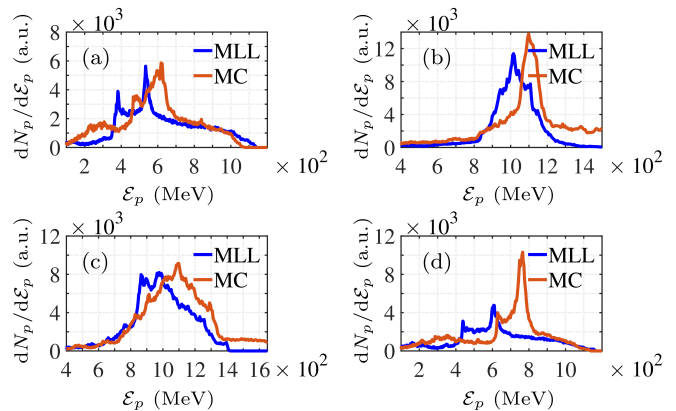


FIG. 6. Proton energy spectra at  $t = 40T_0$ . The pulse duration of the driving laser pulse in (a) is  $\tau_0 = 3T_0$  and (b)  $\tau_0 = 8T_0$ , respectively. The pulse duration of the scattering laser in (c) is  $\tau_1 = 8T_0$  and (d)  $\tau_1 = 25T_0$ , respectively. Other parameters are the same as in Fig. 2.

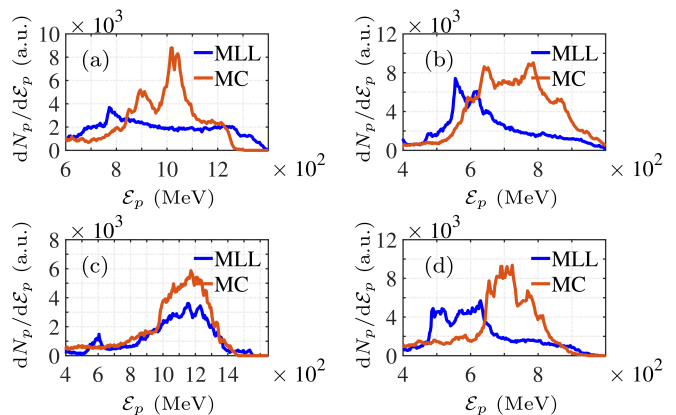


FIG. 7. Proton energy spectra at  $t = 40T_0$ . The scattering laser enters  $\tau_c = 10T_0$  later in (a) and  $10T_0$  earlier in (b), respectively. Initial density of electrons  $n_0 = 250n_c$  and  $350n_c$  in (c) and (d), respectively. Other parameters are the same as in Fig. 2.

the driving laser pulse and the scattered plasma. Consequently, the final difference on the spectra due to SEs is larger, see Fig. 7(b). The role of the target density  $n_0$  is analyzed in Figs. 7(c) and (d). The reduction of the particle number can reduce the acceleration efficiency and also the scattered electron number, thus, SEs are suppressed. For instance, for the case of  $n_0 = 250n_c$ , the signature of SEs cannot be observed easily, see Fig. 7(c). For a higher density target, such as the case of  $n_0 = 350n_c$  in Fig. 7(d), acceleration effects are lower due to the larger target mass and yield lower spectra [47], however, SEs can still be resolved. For much higher densities, much stronger laser pulses are required for acceleration, otherwise, collective RR effects on protons are rather weak.

Besides, we underline that our configuration can also be employed to compress the proton energy spectra, as shown in Fig. 8, in the QRDR (beyond the QRDR, sim-

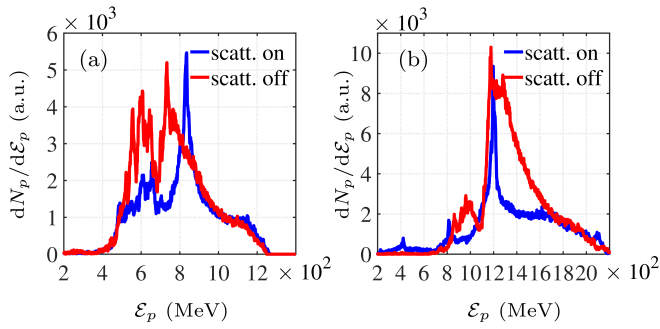


FIG. 8. Spectrum compression effect. (a)  $a_0 \approx 200$ ,  $a_1 \approx 175$ , and  $n_0/n_c = 200$ . (b)  $a_0 \approx 300$ ,  $a_1 \approx 265$ , and  $n_0/n_c = 300$ . The blue and red curves indicate including and excluding the scattering laser pulse. The interaction time delay between the driving laser pulse and the scattering laser pulse is about  $55.7T_0$ . Other parameters are the same as in Fig. 2.

ilar setups have been considered to compress the proton energy spectra [61, 62]). As the front electrons in the accelerated plasma are decelerated or even reflected by the scattering laser pulse due to the radiation energy loss, the front protons are decelerated due to the charge separation force. Consequently, the proton energy spectra are significantly compressed. For instance, in Fig. 8(a) the peak energies without and with the scattering laser pulse are  $E_p \approx 732$  MeV and 835 MeV, respectively, and the scattering laser pulse can significantly compress the energy spreading from 45.5% to 7.9%; in Fig. 8(b), without and with the scattering laser pulse, the peak energies  $E_p \approx 1177$  MeV and 1197 MeV, respectively, and the corresponding energy spreadings are about 23.9% and 4.1%,

which may be very useful for studies and applications of ion acceleration.

## V. CONCLUSION

We have investigated the signature of SEs of photon emission on the proton energy spectra in the interaction of an ultrarelativistic plasma accelerated via RPA head-on colliding with an ultraintense scattering laser pulse in the QRDR. A proper scattering laser pulse can significantly compress the proton spectra. By comparing the simulations of the MLL and MC models, we find that SEs can induce a significant extra shift of the proton energy spectra, which may be quantitatively detected and serve as the signature of SEs. This effects could be measurable with soon achievable ultraintense laser facilities, e.g., the ELI [2].

## VI. ACKNOWLEDGMENT

This work is in part funded by the Science Challenge Project of China (No. TZ2016099), the National Key Research and Development Program of China (Grant No. 2018YFA0404801), and the National Natural Science Foundation of China (Grants Nos. 11874295, 11804269, U1532263, 11875219), and has been performed within the framework of the project High Field Initiative (CZ.02.1.01/0.0/0.0/15 003/0000449) from European Regional Development Fund.

- 
- [1] The Vulcan facility, <http://www.clf.stfc.ac.uk/Pages/The-Vulcan-10-Petawatt-Project.aspx>.
  - [2] The Extreme Light Infrastructure (ELI), <http://www.eli-beams.eu/en/facility/lasers/>.
  - [3] Exawatt Center for Extreme Light Studies (XCELS), <http://www.xcels.iapras.ru/>.
  - [4] V. Yanovsky, V. Chvykov, G. Kalinchenko, P. Rousseau, T. Planchon, T. Matsuoka, A. Maksimchuk, J. Nees, G. Cheriaux, G. Mourou, and K. Krushelnick, *Opt. Express* **16**, 2109 (2008).
  - [5] C. Danson, D. Hillier, N. Hopps, and D. Neely, *High Power Laser Sci. Eng.* **3**, e3 (2015).
  - [6] J. H. Sung, H. W. Lee, J. Y. Yoo, J. W. Yoon, C. W. Lee, J. M. Yang, Y. J. Son, Y. H. Jang, S. K. Lee, and C. H. Nam, *Opt. Lett.* **42**, 2058 (2017).
  - [7] G. Mourou and T. Tajima, *Opt. Photonics News* **22**, 47 (2011).
  - [8] J. Zou, C. Le Blanc, D. Papadopoulos, G. Cheriaux, P. Georges, G. Mennerat, F. Druon, L. Lecherbourg, A. Pellegrina, P. Ramirez, and et al., *High Power Laser Sci. Eng.* **3**, e2 (2015).
  - [9] A. D. Piazza, C. Mller, K. Z. Hatsagortsyan, and C. H. Keitel, *Rev. Mod. Phys.* **84**, 1177 (2012).
  - [10] A. Macchi, M. Borghesi, and M. Passoni, *Rev. Mod. Phys.* **85**, 751 (2013).
  - [11] S. V. Bulanov, T. Z. Esirkepov, D. Habs, F. Pegoraro, and T. Tajima, *Eur. Phys. J. D* **55**, 483 (2009).
  - [12] A. I. Nikishov and V. I. Ritus, *Sov. Phys. JETP* **19**, 529 (1964).
  - [13] T. Erber, *Rev. Mod. Phys.* **38**, 626 (1966).
  - [14] C. S. Shen and D. White, *Phys. Rev. Lett.* **28**, 455 (1972).
  - [15] V. I. Ritus, *J. Russ. Laser Res.* **6**, 497 (1985).
  - [16] J. G. Kirk, A. R. Bell, and I. Arka, *Plasma Phys. Controlled Fusion* **51**, 085008 (2009).
  - [17] I. V. Sokolov, N. M. Naumova, J. A. Nees, G. A. Mourou, and V. P. Yanovsky, *Phys. Plasmas* **16**, 093115 (2009).
  - [18] A. M. Fedotov, N. B. Narozhny, G. Mourou, and G. Korn, *Phys. Rev. Lett.* **105**, 080402 (2010).
  - [19] A. D. Piazza, K. Z. Hatsagortsyan, and C. H. Keitel, *Phys. Rev. Lett.* **105**, 220403 (2010).
  - [20] W. Yan, C. Fruhling, G. G., D. Haden, J. Luo, P. Zhang, B. Zhao, J. Zhang, C. Liu, M. Chen, S. Chen, S. Banerjee, and D. Umstadter, *Nat. Photon.* **11**, 514 (2017).
  - [21] M. Abraham, *Theorie der Elektrizität* (Teubner, Leipzig, 1905).

- [22] H. A. Lorentz, *The Theory of Electrons* (Teubner, Leipzig, 1909).
- [23] P. A. M. Dirac, Proc. Roy. Soc. (London) **A167**, 148 (1938).
- [24] W. Heitler, Math. Proc. Camb. Phil. Soc. **37**, 291 (1941).
- [25] J. Koga, T. Z. Esirkepov, and S. V. Bulanov, *Phys. Plasmas* **12**, 093106 (2005).
- [26] N. Neitz and A. Di Piazza, *Phys. Rev. A* **90**, 022102 (2014).
- [27] N. Neitz and A. Di Piazza, *Phys. Rev. Lett.* **111**, 054802 (2013), 1301.5524.
- [28] J.-X. Li, Y.-Y. Chen, K. Z. Hatsagortsyan, and C. H. Keitel, *Sci. Rep.* **7**, 11556 (2017).
- [29] M. Tamburini, C. H. Keitel, and A. D. Piazza, *Phys. Rev. E* **89**, 021201 (2014).
- [30] A. V. Bashinov, A. V. Kim, and A. M. Sergeev, *Phys. Rev. E* **92**, 043105 (2015).
- [31] H. Y. Wang, X. Q. Yan, and M. Zepf, *Phys. Plasmas* **22**, 093103 (2015).
- [32] T. G. Blackburn, C. P. Ridgers, J. G. Kirk, and A. R. Bell, *Phys. Rev. Lett.* **112**, 015001 (2014).
- [33] C. N. Harvey, A. Gonoskov, A. Ilderton, and M. Marklund, *Phys. Rev. Lett.* **118**, 105004 (2017).
- [34] J.-X. Li, K. Z. Hatsagortsyan, and C. H. Keitel, *Phys. Rev. Lett.* **113**, 044801 (2014).
- [35] Y.-F. Li, Y.-T. Zhao, K. Z. Hatsagortsyan, C. H. Keitel, and J.-X. Li, *Phys. Rev. A* **98**, 052120 (2018).
- [36] T. N. Wistisen, A. D. Piazza, H. V. Knudsen, and U. I. Uggerhøj, *Nat. Commun.* **9**, 795 (2018).
- [37] K. Poder, M. Tamburini, G. Sarri, A. D. Piazza, S. Kuschel, C. Baird, K. Behm, S. Bohlen, J. Cole, D. Corvan, M. Duff, E. Gerstmayr, C. Keitel, K. Krushelnick, S. Mangles, P. McKenna, C. Murphy, Z. Najmudin, C. Ridgers, G. Samarin, D. Symes, A. Thomas, J. Warwick, and M. Zepf, *Phys. Rev. X* **8**, 031004 (2018).
- [38] J. Cole, K. Behm, E. Gerstmayr, T. Blackburn, J. Wood, C. Baird, M. Duff, C. Harvey, A. Ilderton, A. Joglekar, K. Krushelnick, S. Kuschel, M. Marklund, P. McKenna, C. Murphy, K. Poder, C. Ridgers, G. Samarin, G. Sarri, D. Symes, A. Thomas, J. Warwick, M. Zepf, Z. Najmudin, and S. Mangles, *Phys. Rev. X* **8**, 011020 (2018).
- [39] M. Chen, A. Pukhov, T.-P. Yu, and Z.-M. Sheng, *Plasma Phys. Controlled Fusion* **53**, 014004 (2010).
- [40] R. Capdessus and P. McKenna, *Phys. Rev. E* **91**, 053105 (2015).
- [41] M. Tamburini, F. Pegoraro, A. D. Piazza, C. H. Keitel, and A. Macchi, *New J. Phys.* **12**, 123005 (2010).
- [42] J. Limpouch, N. N. Demchenko, S. Y. Gus'kov, M. Kálal, A. Kasperczuk, V. N. Kondrashov, E. Krouský, K. Masek, P. Pisarczyk, T. Pisarczyk, and V. B. Rozanov, *Plasma Phys. Controlled Fusion* **46**, 1831 (2004).
- [43] A. E. Bugrov, I. N. Burdonskiy, O. L. Dedova, I. K. Fasakhov, V. V. Gavrilov, A. Y. Goltsov, A. I. Gromov, V. N. Kondrashov, S. N. Koptyaev, N. G. Kovalskii, and S. F. Medovshchikov, *Contrib. Plasma Phys.* **45**, 185 (2005).
- [44] P. Hilz, T. M. Ostermayr, A. Huebl, V. Bagnoud, B. Borm, M. Bussmann, M. Gallei, J. Gebhard, D. Haffa, J. Hartmann, T. Kluge, F. H. Lindner, P. Neumayr, C. G. Schaefer, U. Schramm, P. G. Thirolf, T. F. Rsch, F. Wagner, B. Zielbauer, and J. Schreiber, *Nat. Commun.* **9**, 423 (2018).
- [45] A. Macchi, F. Cattani, T. V. Liseykina, and F. Cornolti, *Phys. Rev. Lett.* **94**, 165003 (2005).
- [46] X. Q. Yan, C. Lin, Z. M. Sheng, Z. Y. Guo, B. C. Liu, Y. R. Lu, J. X. Fang, and J. E. Chen, *Phys. Rev. Lett.* **100**, 135003 (2008).
- [47] B. Qiao, M. Zepf, M. Borghesi, B. Dromey, M. Geissler, A. Karmakar, and P. Gibbon, *Phys. Rev. Lett.* **105**, 155002 (2010).
- [48] S. V. Bulanov, E. Y. Echkina, T. Z. Esirkepov, I. N. Inovenkov, M. Kando, F. Pegoraro, and G. Korn, *Phys. Rev. Lett.* **104**, 135003 (2010).
- [49] T. Esirkepov, M. Borghesi, S. V. Bulanov, G. Mourou, and T. Tajima, *Phys. Rev. Lett.* **92**, 175003 (2004).
- [50] F. Pegoraro and S. V. Bulanov, *Phys. Rev. Lett.* **99**, 065002 (2007).
- [51] X. Wang, R. Zgadza, N. Fazel, Z. Li, S. A. Yi, X. Zhang, W. Henderson, Y.-Y. Chang, R. Korzekwa, H.-E. Tsai, C.-H. Pai, H. Quevedo, G. Dyer, E. Gaul, M. Martinez, A. C. Bernstein, T. Borger, M. Spinks, M. Donovan, V. Khudik, G. Shvets, T. Ditmire, and M. C. Downer, *Nat. Commun.* **4**, 1988 (2013).
- [52] W. P. Leemans, A. J. Gonsalves, H.-S. Mao, K. Nakamura, C. Benedetti, C. B. Schroeder, C. Tóth, J. Daniels, D. E. Mittelberger, S. S. Bulanov, J.-L. Vay, C. G. R. Geddes, and E. Esarey, *Phys. Rev. Lett.* **113**, 245002 (2014).
- [53] B. Wolter, M. G. Pullen, A. T. Le, M. Baudisch, K. Doblhoff-Dier, A. Senftleben, M. Hemmer, C. D. Schroter, J. Ullrich, T. Pfeifer, R. Moshhammer, S. Grafe, O. Vendrell, C. D. Lin, and J. Biegert, *Science* **354**, 308 (2016).
- [54] R. P. Chatelain, V. R. Morrison, B. L. M. Klarenaar, and B. J. Siwick, *Phys. Rev. Lett.* **113**, 235502 (2014).
- [55] C. P. Ridgers, C. S. Brady, R. Ducloux, J. G. Kirk, K. Bennett, T. D. Arber, A. P. L. Robinson, and A. R. Bell, *Phys. Rev. Lett.* **108**, 165006 (2012).
- [56] T. D. Arber, K. Bennett, C. S. Brady, A. Lawrence-Douglas, M. G. Ramsay, N. J. Sircombe, P. Gillies, R. G. Evans, H. Schmitz, A. R. Bell, and C. P. Ridgers, *Plasma Phys. Control. Fusion* **57**, 113001 (2015).
- [57] N. V. Elkina, A. M. Fedotov, I. Y. Kostyukov, M. V. Legkov, N. B. Narozhny, E. N. Nerush, and H. Ruhl, *Phys. Rev. Spec. Top. Accel Beams* **14**, (2011).
- [58] C. Ridgers, J. Kirk, R. Ducloux, T. Blackburn, C. Brady, K. Bennett, T. Arber, and A. Bell, *J. Comput. Phys.* **260**, 273 (2014).
- [59] D. Green and C. Harvey, *Comput. Phys. Commun.* **192**, 313 (2015).
- [60] A. Gonoskov, S. Bastrakov, E. Efimenko, A. Ilderton, M. Marklund, I. Meyerov, A. Muraviev, A. Sergeev, I. Surmin, and E. Wallin, *Phys. Rev. E* **92**, 023305 (2015).
- [61] Y. Wan, C. J. Zhang, F. Li, Y. P. Wu, J. F. Hua, C. H. Pai, W. Lu, Y. Q. Gu, C. Joshi, and W. B. Mori, <http://arxiv.org/abs/1707.07290v1>.
- [62] W. Zhou, X. Hong, B. Xie, Y. Yang, L. Wang, J. Tian, R. Tang, and W. Duan, *Phys. Rev. Accel. Beams* **21**, 021301 (2018).
- [63] L. D. Landau and E. M. Lifshitz, in *The Classical Theory of Fields* (Oxford:Elsevier, 1975) Chap. 76, 2nd ed.
- [64] I. V. Sokolov, J. A. Nees, V. P. Yanovsky, N. M. Naumova, and G. A. Mourou, *Phys. Rev. E* **81**, 036412 (2010).



- [65] M. K. Khokonov and I. Z. Bekulova, *Tech. Phys.* **55**, 728 (2010).
- [66] F. Rohrlich, *Phys. Rev. E* **77**, 046609 (2008).
- [67] R. T. Hammond, *Phys. Rev. A* **81**, 062104 (2010).
- [68] S. V. Bulanov, T. Z. Esirkepov, M. Kando, J. K. Koga, and S. S. Bulanov, *Phys. Rev. E* **84**, 056605 (2011).
- [69] A. G. R. Thomas, C. P. Ridgers, S. S. Bulanov, B. J. Griffin, and S. P. D. Mangles, *Phys. Rev. X* **2**, 041004 (2012).
- [70] S. Kar, K. F. Kakolee, B. Qiao, A. Macchi, M. Cerchez, D. Doria, M. Geissler, P. McKenna, D. Neely, J. Osterholz, R. Prasad, K. Quinn, B. Ramakrishna, G. Sarri, O. Willi, X. Y. Yuan, M. Zepf, and M. Borghesi, *Phys. Rev. Lett.* **109**, 185006 (2012).
- [71] I. J. Kim, K. H. Pae, C. M. Kim, H. T. Kim, J. H. Sung, S. K. Lee, T. J. Yu, I. W. Choi, C.-L. Lee, K. H. Nam, P. V. Nickles, T. M. Jeong, and J. Lee, *Phys. Rev. Lett.* **111**, 165003 (2013).
- [72] X. S. Geng, L. L. Ji, B. F. Shen, B. Feng, Z. Guo, Q. Yu, L. G. Zhang, and Z. Z. Xu, <http://arxiv.org/abs/1811.04741v2>.